Int J Clin Exp Pathol 2026;19(1):39-53
www.ijcep.com /ISSN:1936-2625/IJCEP0168690

Original Article

Integrated bioinformatic analysis of biomarkers, pathways, and immune cell infiltration in ossification of the ligamentum flavum

Chuanhong Dou, Fengzhen Zhang, Wenhao Wang, Ruijie Liu, Shaobo Lu, Changliang Peng

Department of Spinal Surgery, The Second Qilu Hospital of Shandong University, Jinan, Shandong, China

Received September 9, 2025; Accepted December 22, 2025; Epub January 15, 2026; Published January 30, 2026

Abstract: Background: Ossification of the ligamentum flavum (OLF) represents a pathologic condition contributing to spinal stenosis. Its underlying molecular mechanisms have not been fully elucidated. The present study aimed to identify gene expression alterations and associated molecular pathways in OLF through comprehensive bioinformatic analysis. Methods: Gene expression profiles from GSE113212 were analyzed to identify differentially expressed genes (DEGs) between OLF and non-OLF tissues. Functional enrichment was assessed by GO and KEGG analyses. A protein-protein interaction (PPI) network was constructed to screen hub genes, while immune cell infiltration was quantified using CIBERSORT. Gene Set Variation Analysis (GSVA) and Gene Set Enrichment Analysis (GSEA) were employed to explore pathway-level dysregulation. Results: A total of 148 DEGs were identified, including 118 downregulated and 30 upregulated genes in OLF tissues compared to non-OLF controls. Functional analyses revealed significant enrichment in muscle contraction-related processes, immune responses, and cytokine-cytokine receptor interactions. FN1, EGFR, and ACTA1 were identified as key hub genes. GSEA highlighted the activation of epithelial-mesenchymal transition (EMT), glycolysis, and inflammatory responses pathways in OLF. Immune infiltration analysis demonstrated distinct alterations in dendritic cells, macrophages, and eosinophils, with hub genes exhibiting strong correlations with specific immune cell subsets. Conclusion: This study uncovered possible molecular mechanisms driving OLF, emphasizing the interplay between immune-related pathways and key fibrotic regulators (FN1, EGFR, and ACTA1). These findings offer novel insight into the immune microenvironment of OLF and suggest potential targets for therapeutic intervention.

Keywords: Ossification of ligamentum flavum, differentially expressed genes, biomarker, immune cells infiltration, bioinformatics analysis

Introduction

Ossification of the ligamentum flavum (OLF) is a degenerative spinal disorder predominantly observed in East Asian populations, particularly among middle-aged and elderly individuals [1, 2]. The thoracic variant (TOLF) characteristically involves the lower thoracic spine, leading to thoracic spinal stenosis and progressive spinal cord compression. Clinical manifestations include lower extremity motor weakness, sensory deficits, gait disturbances, and bladder dysfunction, all of which severely impair a patient's quality of life [3, 4]. Currently, surgical decompression remains the gold standard treatment for TOLF [5, 6]. Nevertheless, surgical intervention carries considerable risks, with neurological injury and cerebrospinal fluid leakage representing the most frequently encountered complications [6, 7]. Clinicians face challenges in diagnosing and treating this disease, as there are currently no effective strategies to halt or slow the progression of TOLF due to its uncertain pathogenesis [8, 9]. Therefore, elucidating the underlying mechanism of OLF is needed to identify therapeutic targets. OLF is a complex, multifactorial disease influenced by both hereditary and environmental factors, including genetic predisposition, mechanical stress, chronic inflammation, infection, and metabolic disorders, all of which contribute to disease susceptibility [8, 9]. Despite accumu-

https://doi.org/10.62347/ELFC5188

lating evidence, the precise molecular mechanisms underlying the onset and progression of OLF remain largely unknown.

The immune response plays a pivotal role in the pathogenesis of various human diseases, including chronic inflammation, tumorigenesis, and viral infection. Activated immune cells such as neutrophils, monocytes, macrophages, mast cells, T cells, and dendritic cells are implicated as key mediators in tissue repair, remodeling, and fibrosis [10, 11]. Recent studies have provided novel insight into the pathogenesis of OLF by elucidating the role of immune cell infiltration in driving the inflammatory response [12-14]. For instance, previous studies have identified a chronic inflammatory microenvironment within OLF tissues, characterized by substantial infiltration of immune cells, particularly macrophages [15, 16]. Furthermore, specific pro-inflammatory cytokines, such as tumor necrosis factor-alpha (TNF-α) and transforming growth factor-beta (TGF-β), have been implicated in promoting the pathologic ossification process [17, 18]. However, the precise molecular mechanisms underlying the immune-inflammatory response in OLF remain poorly understood. Therefore, comprehensive investigation of immune cell infiltration patterns and within ossified ligamentum flavum is crucial for identifying safe and effective diagnostic biomarkers and therapeutic targets.

In this study, we retrieved gene expression data from patients with OLF from the Gene Expression Omnibus (GEO) database and performed comprehensive bioinformatic analyses. First, we conducted an analysis to identify differentially expressed genes (DEGs) between OLF and non-OLF samples, followed by functional enrichment and signaling pathway analyses. Subsequently, we employed immune cell infiltration analysis using the CIBERSORT algorithm to characterize the composition and abundance of immune cell populations in OLF tissues compared to healthy controls. Finally, we systematically investigated the correlations among DEGs, enriched signaling pathways, and infiltrating immune cell infiltration to elucidate their potential roles in OLF pathogenesis. Collectively, our findings provide novel insight into the immune-regulatory mechanisms involved in the pathogenesis of OLF, which may facilitate the identification of diagnostic biomarkers and therapeutic targets.

Materials and methods

Microarray dataset acquisition and description

Gene expression profiles were retrieved from the GSE113212 dataset available in the GEO database (http://www.ncbi.nlm.nih.gov/geo) [19]. The GSE113212 dataset, submitted by Masatoshi Morimoto et al., was generated using the GPL17077 platform (Agilent-039494 SurePrint G3 Human GE v2 8x60K Microarray 039381) and comprises eight human ligamentum flavum samples. These samples are categorized into two groups: four samples annotated as “Flavum_young” (aged 19-24 years, representing non-hypertrophic ligamentum flavum from young individuals) and four samples annotated as “Flavum_elderly” (aged 75-83 years, representing hypertrophic ligamentum flavum from elderly patients).

Study design and sample selection

We conducted a comprehensive secondary analysis of this publicly available dataset. The inclusion criteria were defined as follows: (1) samples belonging to the GSE113212 series; (2) samples derived from human ligamentum flavum tissue; and (3) availability of complete and high-quality gene expression data on the GPL17077 platform. Based on these criteria, the case group consisted of the four elderly hypertrophic ligamentum flavum samples (“Flavum_elderly”), while the control group comprised the four young non-hypertrophic ligamentum flavum samples (“Flavum_young”). The exclusion criteria were established to ensure data quality and relevance: (1) samples not derived from human ligamentum flavum tissue; (2) samples from non-human organisms; and (3) samples with incomplete, corrupted, or missing gene expression data.

Rationale for sample classification

Given the well-established pathologic association between ligamentum flavum hypertrophy and ossification of the ligamentum flavum (OLF), wherein hypertrophy is considered a precursor or concurrent feature of OLF [20], the hypertrophic elderly ligamentum flavum samples in GSE113212 were designated as representative of the OLF phenotype in the present analysis. This classification is supported by previous studies demonstrating that age-related

hypertrophic changes in the ligamentum flavum share similar molecular and cellular characteristics with OLF pathology [8, 21-23].

Data processing and identification of differentially expressed genes

DEGs were identified through comparative transcriptomic analysis of OLF and non-OLF tissue samples from the GSE113212 dataset using GEO2R (http://www.ncbi.nlm.nih.gov/geo/geo2r/) [19], an interactive web-based analytical tool that implements the limma R package for statistical analysis. The eight ligamentum flavum samples were stratified into two groups based on the original dataset annotations: the OLF group (n = 4, "Flavum_elderly") and the non-OLF control group (n = 4, "Flavum_young"). Raw expression data were subjected to quantile normalization and log2-transformation using the default parameters of GEO2R to ensure data comparability and reduce technical variation. Quality control procedures were implemented to exclude probes lacking official gene symbols or containing missing expression values. When multiple probes corresponded to the same gene symbol, the probe with the largest absolute $\log_2$ fold change ($|\log_2 FC|$) was retained to represent that gene. For each probe, GEO2R employed a linear modeling approach to calculate the $\log_2 FC$ and corresponding *p*-value for differential expression between OLF and non-OLF tissues. Genes satisfying the dual criteria of $|\log_2 FC| \geq 3.00$ and *p*-value < 0.05 were designated as statistically significant DEGs. To comprehensively visualize the expression patterns and distribution of DEGs between the two groups, we generated heatmaps to display hierarchical clustering of gene expression profiles, volcano plots to illustrate the magnitude and statistical significance of differential expression, and bar charts to summarize the numbers of upregulated and downregulated genes.

Function enrichment analysis of DEGs

To elucidate the biological functions and molecular pathways associated with the identified DEGs, we performed comprehensive functional enrichment analysis using the Database for Annotation, Visualization, and Integrated Discovery (DAVID, http://david.abcc.ncifcrf.gov/) [24]. Gene Ontology (GO) enrichment analysis was conducted to categorize DEGs into three functional domains: biological process (BP), molecular function (MF), and cellular component (CC) [25]. Concurrently, Kyoto Encyclopedia of Genes and Genomes (KEGG) pathway analysis was performed to identify significantly enriched signaling pathways and metabolic processes. For both GO and KEGG analyses, statistical significance was defined as $P < 0.05$, and only terms or pathways meeting this threshold were considered significantly enriched. The top five enriched GO terms in each category (BP, MF, and CC) and the most significantly enriched KEGG pathways were selected for visualization and further interpretation.

Protein-protein interaction (PPI) network construction and hub genes identification

Protein-protein interactions (PPIs) are fundamental to understanding the coordinated molecular mechanisms underlying ligamentum flavum ossification. In OLF, critical processes such as extracellular matrix (ECM) remodeling, inflammatory activation, and osteogenic differentiation are orchestrated by complex networks of interacting proteins rather than individual genes acting in isolation. Therefore, constructing a PPI network of DEGs can facilitate the identification of central regulatory nodes in OLF pathogenesis. The Search Tool for the Retrieval of Interacting Genes (STRING, http://string.embl.de/) database [26] was employed to construct the PPI network using the identified DEGs, with a confidence score threshold of ≥ 0.7. The network was visualized and analyzed using Cytoscape software, and hub genes were identified based on a degree centrality threshold of ≥ 15. To comprehensively characterize hub gene importance, five complementary centrality metrics (Closeness, Betweenness, Radiality, BottleNeck, and Stress) were calculated using the Cytohubba plugin [27, 28]. Genes consistently ranked highly across all five algorithms were designated as key hub genes for further analysis.

Gene Set Variation Analysis (GSVA)

To evaluate systematically the pathway-level differences in biological processes between OLF and non-OLF samples, we performed GSVA [29], a non-parametric and unsupervised method for assessing gene set enrichment across sample expression profiles. Gene sets representing well-defined biological pathways and

processes were retrieved from the Molecular Signatures Database (MSigDB; http://software.broadinstitute.org/gsea/msigdb/index.jsp) [29]. The GSVA algorithm was then applied to calculate enrichment scores for each gene set in individual samples, thereby transforming gene-level expression data into pathway-level enrichment scores. This transformation enables the quantitative assessment of biological pathway activity and facilitates the identification of functionally relevant pathways that differ between OLF and non-OLF tissues. By converting gene expression variations into pathway-level changes, GSVA provides a comprehensive framework for evaluating the biological functional states of samples and identifying key pathways associated with OLF pathogenesis. Differentially enriched pathways between the two groups were visualized using heatmaps, with statistical significance determined by appropriate comparative analysis.

Gene Set Enrichment Analysis (GSEA)

To identify coordinated pathway-level changes between OLF and non-OLF tissues, GSEA was performed using GSEA software (Version 4.2.3; https://www.gsea-msigdb.org/gsea/index.jsp) [30]. GSEA evaluates whether predefined gene sets show statistically significant, concordant differences between the two biological states by analyzing the entire ranked gene list rather than focusing solely on individual differentially expressed genes. Genes were ranked using the Signal2Noise metric, which measures the difference in mean expression between phenotypes relative to standard deviation. The analysis was conducted with 1,000 permutations using the 'phenotype' permutation type. Gene sets containing between 15 and 500 genes were included to ensure reliable statistical analysis. The hallmark gene set collection (h.all.v7.1.symbols.gmt) from the MSigDB [31, 32] was used as the reference. Significantly enriched gene sets were identified based on the following criteria: normalized enrichment score (NES) > 0.6, nominal *P*-value < 0.05, and false discovery rate (FDR) q-value < 0.25.

Immune cell infiltration analysis

To characterize the immune microenvironment in OLF tissues, immune cell infiltration analysis was performed using single-sample gene set enrichment analysis (ssGSEA) and the CIBERSORT algorithm [33]. CIBERSORT was employed to quantify the relative proportions of 22 distinct immune cell types in each sample using the CIBERSORT platform (https://cibersortx.stanford.edu/) [34] with the LM22 signature matrix. Only samples with CIBERSORT *P*-values < 0.05 were retained for analysis to ensure reliable deconvolution results. Correlation analysis among the 22 immune cells types was performed using Pearson correlation coefficients, and the results were visualized using heatmaps generated by the Sangerbox platform (http://vip.sangerbox.com/home.html) [35]. To investigate the relationships between hub genes (FN1, EGFR, and ACTA1) and the immune microenvironment, Pearson correlation analysis was conducted between hub gene expression levels and immune cell abundances. Correlations were considered significant if they met the criteria of $|r| > 0.3$ and $P < 0.05$.

Results

Identification of DEGs

Differential gene expression analysis of the GSE113212 dataset, comparing OLF tissues (n = 4) with non-OLF controls (n = 4), identified a total of 148 DEGs using the criteria of $|\log_2 FC| \geq 3.00$ and *P*-value < 0.05 (**Table 1**). The expression patterns of these DEGs were visualized through a heatmap (**Figure 1A**) and a volcano plot (**Figure 1B**), demonstrating distinct transcriptomic profiles between the two groups. Among the 148 DEGs, 118 genes (79.7%) were significantly downregulated, while 30 genes (20.3%) were significantly upregulated in OLF tissues compared to controls (**Table 1**; **Figure 1C**). The upregulated genes included FN1, IL11, CCL3, MMP1, and TNFSF11, which are associated with ECM remodeling, inflammation, and osteogenesis. The downregulated genes were enriched for muscle-related genes (ACTA1, MYH1/2/7, TNNT1, and CKM) and immune-related genes (EGFR, PTPRC, CD3E, and CD86), suggesting complex transcriptomic reprogramming in OLF pathogenesis.

GO and KEGG pathway enrichment analysis

To elucidate the biological functions of the 148 DEGs, functional enrichment analysis of the DEGs was conducted using the DAVID web tool. GO analysis categorized the DEGs into BP, MF, and CC domains (P < 0.05). GO biological process analysis revealed significant enrichment in muscle contraction, skeletal muscle contrac-

Table 1. Identification of 148 DEGs associated with OLF

Regulation	Gene name
Upregulated (n = 30)	ULBP1, GABRD, KIAA1751, LY6D, COL2A1, CHRDL2, IL11, PVRL4, NXPH4, SBSN, FN1, CYTL1, CCL3, CYP27C1, CCL3L3, CA9, CRTAC1, TREM2, CLEC3A, TNFSF11, AMTN, SOX11, RN5-8S1, CCL18, CLEC18C, MMP1, C10orf81, SYT13, CRLF1, CBLN4
Downregulated (n = 118)	MYADML, FGFR1OP2, C9orf117, C6orf138, JPH4, BTC, GIGYF2, IL2RA, JSRP1, FEM1A, LRRC10, ADARB2, JAKMIP2, WNT2B, CA5BP1, SPTY2D1, TGM6, NUDCD3, ZNF620, COG8, BTN3A1, FLJ42842, CISH, PIK3R5, FLG, WDR67, EGFR, FMR1NB, TTLL9, C1orf61, CTNND1, PPAN-P2RY11, ATXN3L, KCNIP1, GPR17, EFTUD1, AKAP12, AANAT, CCDC150, RTKN2, FAM160A1, ZCCHC13, OR52I2, RNF150, SLC10A1, REP15, TEF, RALYL, C13orf30, CDRT15L2, DHRS4L1, DCDC2, DPRX, BCR, WDR33, TTC23, TEX12, ZNF806, GRIK3, PPP1R1A, FTO, BICC1, PTPRC, OR52E8, TMEM52, Q5A5F0, CCDC66, FGA, IFT74, CALCA, XRRA1, C4orf51, OSTBETA, XAGE-4, SMARCA4, CD3E, MAGEB6, MGC39584, GPR182, KRT79, RPA4, PROM2, NDP, RAP1GAP, GPR179, ACTA1, PPP6R1, PNMT, SPEN, LRRC2, CKM, HMBOX1, CPNE9, MYOT, PPP1R1B, VPS18, CD86, MYH7, MYL1, MB, MYH2, MYH1, SLCO1B3, ATP2A1, PLK5, NRAP, TNNT1, MYLPF, BCAS1, TCAP, TNNC1, XIRP2, EEF1A2, SYNPO2L, CSRP3, LMOD3, CNIH2, FLJ41350

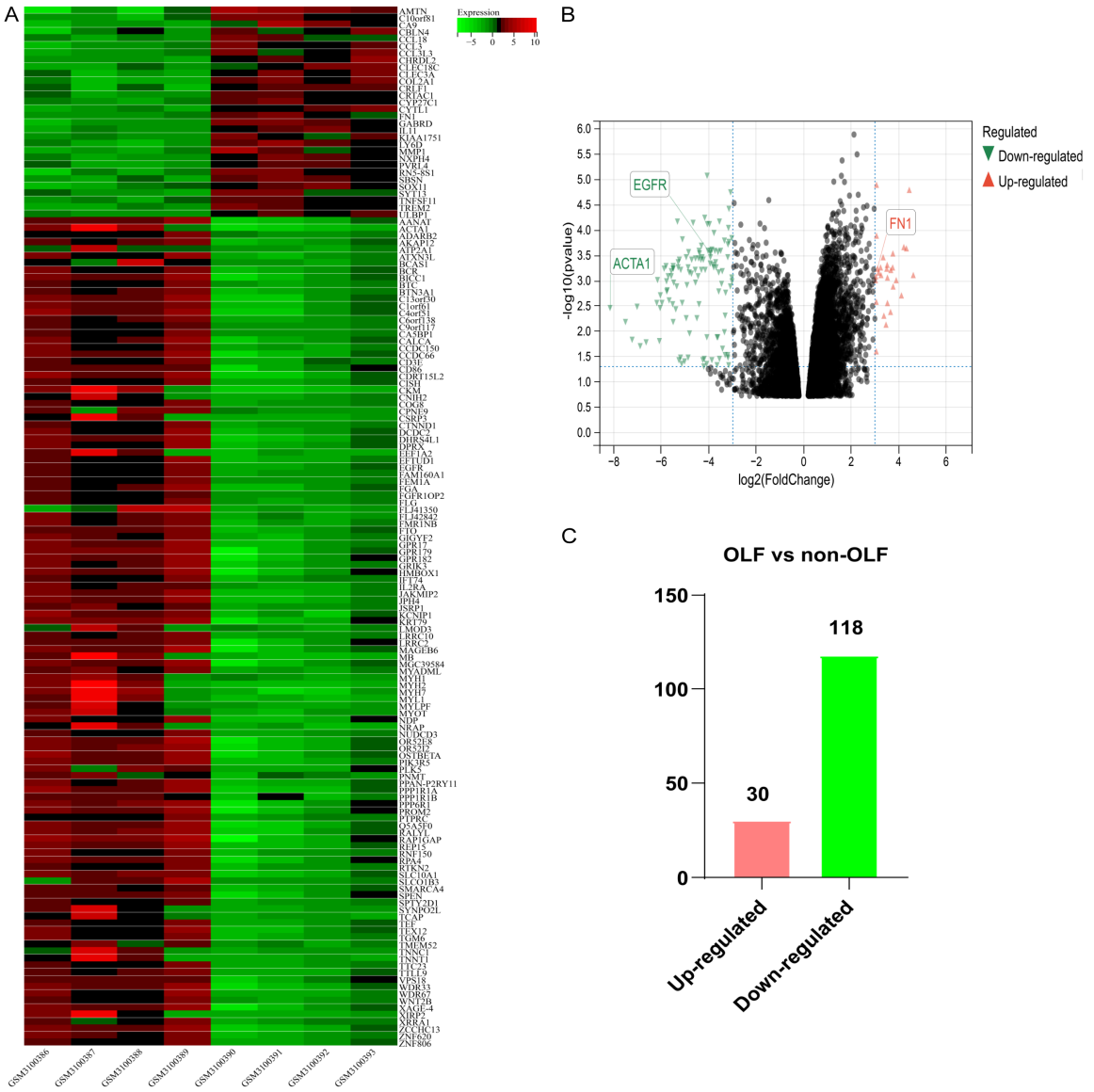

Figure 1. Identification of differentially expressed genes (DEGs) in OLF and non-OLF samples. A. Heatmap displays the expression profiles of 148 identified DEGs, showing clear differences between non-OLF and OLF samples (n = 4 per group). B. Volcano plot illustrates the overall distribution of DEGs, with significantly upregulated (red dots) and downregulated (green dots) genes highlighted. C. Bar chart shows that 148 DEGs were identified in the GSE113212 dataset, comprising 118 downregulated and 30 upregulated genes in OLF samples.

Table 2. The top five enriched GO terms identified among the 148 DEGs associated with OLF

Category	Description	Count	*P*-value
BP	muscle contraction	8	1.15E-06
BP	skeletal muscle contraction	5	2.03E-05
BP	muscle filament sliding	4	9.39E-05
BP	sarcomere organization	5	9.93E-05
BP	monocyte chemotaxis	5	1.58E-04
CC	muscle myosin complex	4	9.35E-05
CC	Z disc	7	1.81E-04
CC	sarcomere	5	2.20E-04
CC	myosin II complex	4	4.00E-04
CC	extracellular space	25	7.87E-04
MF	actin binding	9	0.001
MF	structural constituent of muscle	4	0.002
MF	actin filament binding	7	0.003
MF	receptor binding	9	0.004
MF	alpha-actinin binding	3	0.004
KEGG	Rheumatoid arthritis	6	2.26E-04
KEGG	Motor proteins	7	9.93E-04
KEGG	Adrenergic signaling in cardiomyocytes	5	0.013
KEGG	Viral protein interaction with cytokine and cytokine receptor	4	0.022
KEGG	Cytokine-cytokine receptor interaction	6	0.032

tion, muscle filament sliding, sarcomere organization, and monocyte chemotaxis (**Table 2**; **Figure 2A**). Molecular function analysis showed significant enrichment in actin binding, structural constituent of muscle, actin filament binding, receptor binding, and alpha-actinin binding (**Table 2**; **Figure 2B**). Cellular component analysis indicated that DEGs were primarily localized to the muscle myosin complex, Z disc, sarcomere, myosin II complex, and extracellular space (**Table 2**; **Figure 2C**).

KEGG pathway analysis identified five significantly enriched pathways ($P < 0.05$), including rheumatoid arthritis, motor proteins, adrenergic signaling in cardiomyocytes, viral protein interaction with cytokines and cytokine receptors, and cytokine-cytokine receptor interaction (**Table 2**; **Figure 2D**). These findings indicated that OLF is characterized by downregulation of muscle contractile genes and activation of inflammatory and immune-related pathways.

GSEA and GSVA analysis

To evaluate pathway-level changes in OLF, GSEA was performed using GSEA software [19, 24] on the entire ranked gene expression dataset from OLF (n = 4) and non-OLF (n = 4) samples. Of the 49 hallmark gene sets analyzed, 38 (77.6%) showed increased activity in OLF samples, with 9 gene sets (18.4%) exhibiting significant enrichment at FDR q-value < 0.25. In contrast, 11 gene sets (22.4%) showed increased activity in the controls, with 5 (10.2%) significantly enriched. The top seven significantly enriched gene sets in OLF samples (**Table 3**; **Figure 3A-G**) included: HALLMARK_EPITHELIAL_MESENCHYMAL_TRANSITION (NES = 2.05, FDR = 1.15×10^{-6}), HALLMARK_GLYCOLYSIS (NES = 2.01, FDR = 2.03×10^{-5}), HALLMARK_CHOLESTEROL_HOMEOSTASIS (NES = 1.80, FDR = 9.39×10^{-5}), HALLMARK_IL6_JAK_STAT3_SIGNALING (NES = 1.77, FDR = 9.93×10^{-5}), HALLMARK_ANDROGEN_RESP-

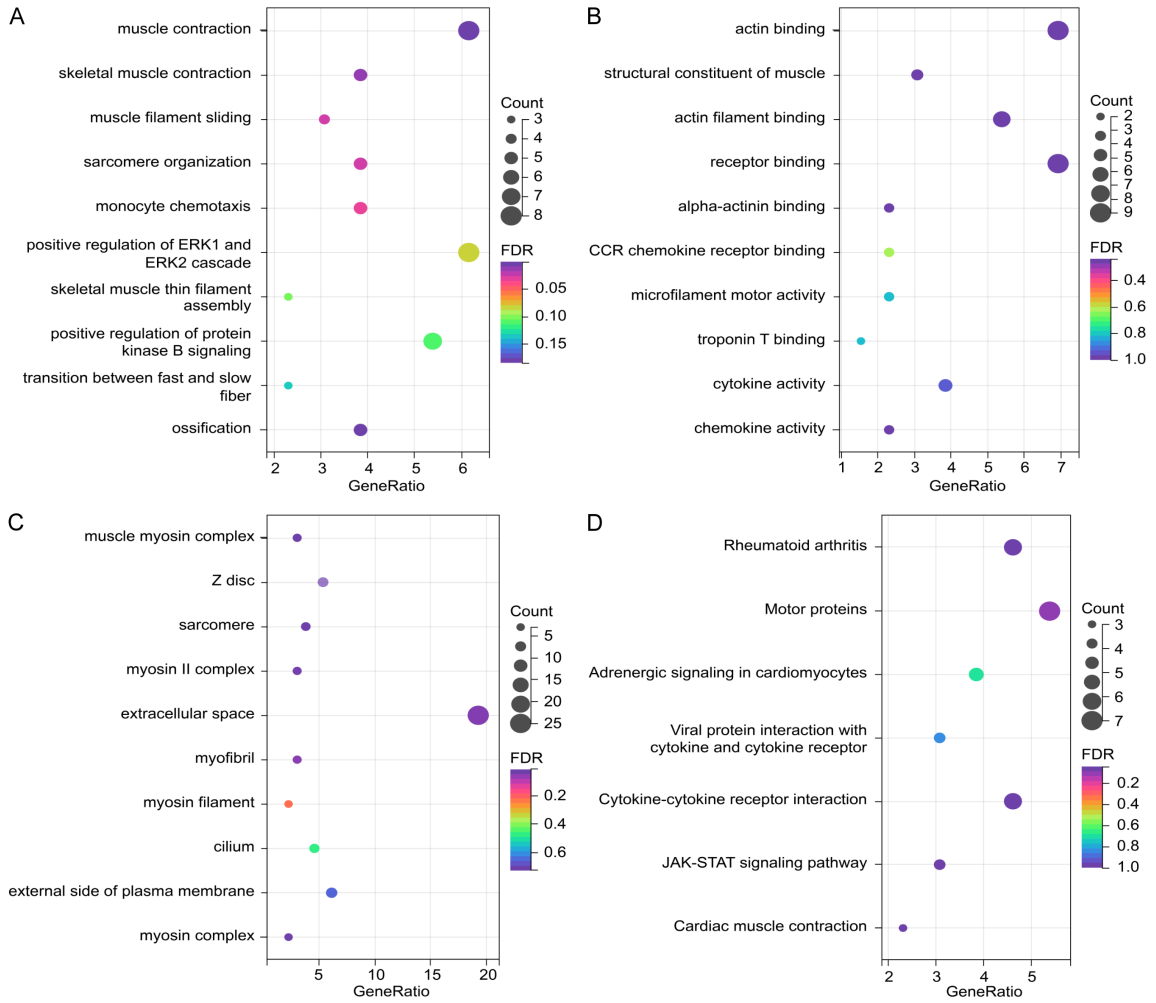

Figure 2. GO and KEGG pathway enrichment analysis of DEGs. A. Biological processes (BP) analysis revealed that DEGs were predominantly enriched in terms related to muscle contraction, sarcomere organization, and monocyte chemotaxis. B. Molecular function (MF) analysis highlighted significant associations with actin binding and structural constituents of muscle. C. Cellular component (CC) analysis indicated that the DEGs were primarily localization to the muscle myosin complex and sarcomere. D. KEGG pathway analysis demonstrated significant enrichment in signaling pathways such as Rheumatoid arthritis and Adrenergic signaling in cardiomyocytes.

Table 3. GSEA results showing the top 7 gene sets enriched in the OLF phenotype

Description	NES	NOM *p*-value	FDR q-value
HALLMARK_EPITHELIAL_MESENCHYMAL_TRANSITION	2.05	0	1.15E-06
HALLMARK_GLYCOLYSIS	2.01	0	2.03E-05
HALLMARK_CHOLESTEROL_HOMEOSTASIS	1.80	0	9.39E-05
HALLMARK_IL6_JAK_STAT3_SIGNALING	1.77	0.001	9.93E-05
HALLMARK_ANDROGEN_RESPONSE	1.63	0.01	1.58E-04
HALLMARK_INFLAMMATORY_RESPONSE	1.58	0.005	9.35E-05
HALLMARK_HYPOXIA	1.56	0.003	1.81E-04

ONSE (NES = 1.63, FDR = 1.58×10^{-4}), HALLMARK_INFLAMMATORY_RESPONSE (NES = 1.58, FDR = 9.35×10^{-5}), and HALLMARK_HYPOXIA (NES = 1.56, FDR = 1.81×10^{-4}). These findings indicated that OLF is characterized by activation of EMT, metabolic reprogramming, inflammatory signaling, and hypoxia response pathways.

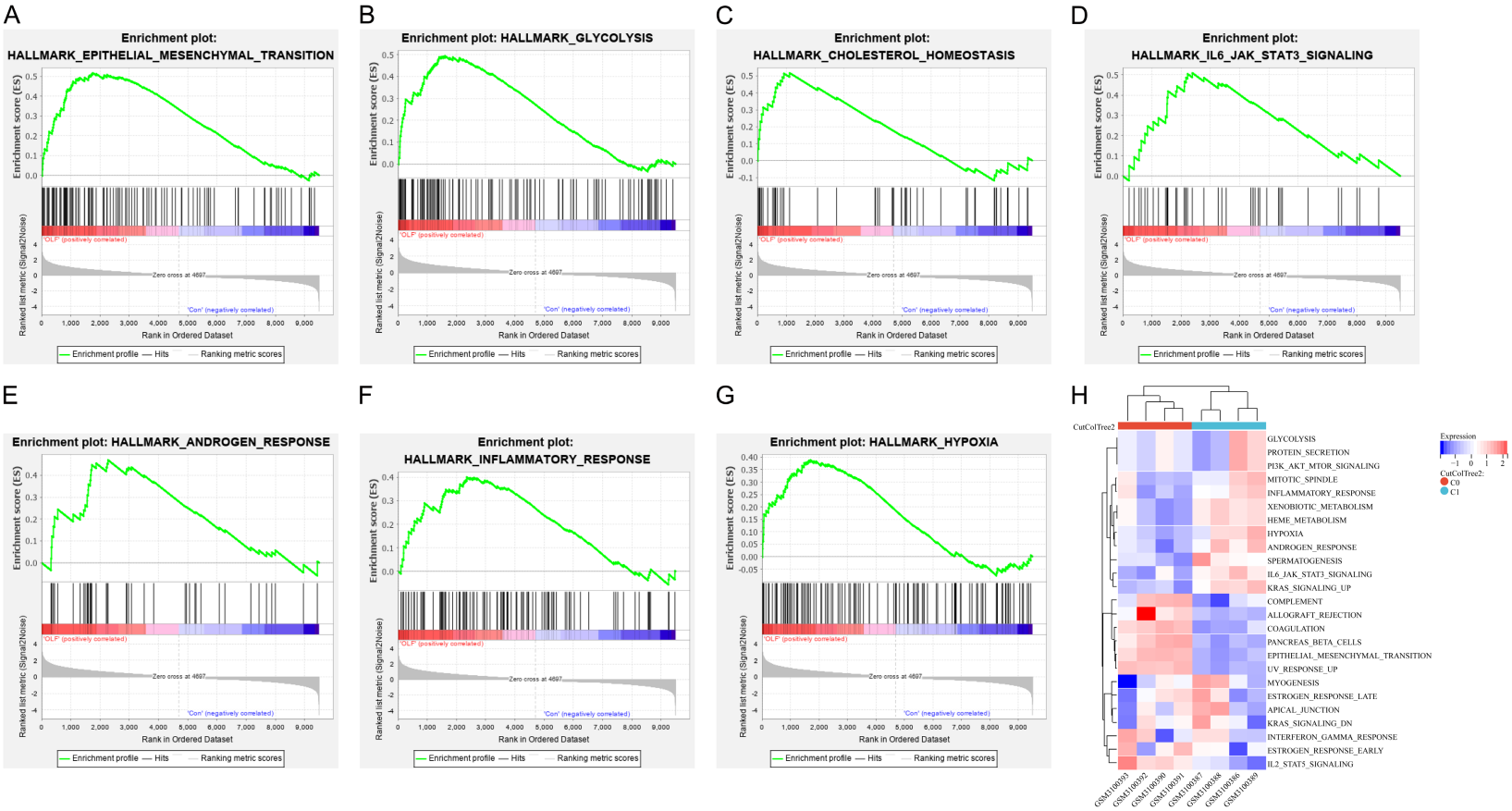

Figure 3. GSEA and GSVA analyses of pathway activity in OLF and non-OLF samples. (A-G) GSEA identified significant enrichment of several gene sets in OLF samples compared to non-OLF samples. (A) HALLMARK_EPITHELIAL_MESENCHYMAL_TRANSITION, (B) HALLMARK_GLYCOLYSIS, (C) HALLMARK_CHOLESTEROL_HOMEOSTASIS, (D) HALLMARK_IL6_JAK_STAT3_SIGNALING, (E) HALLMARK_ANDROGEN_RESPONSE, (F) HALLMARK_INFLAMMATORY_RESPONSE, and (G) HALLMARK_HYPOXIA. (H) GSVA analysis further distinguished the pathway activity between the two groups, revealing significant differential enrichment in pathways such as glycolysis, PI3K/AKT/mTOR, mitotic spindle, and IL6/JAK/STAT3 signaling.

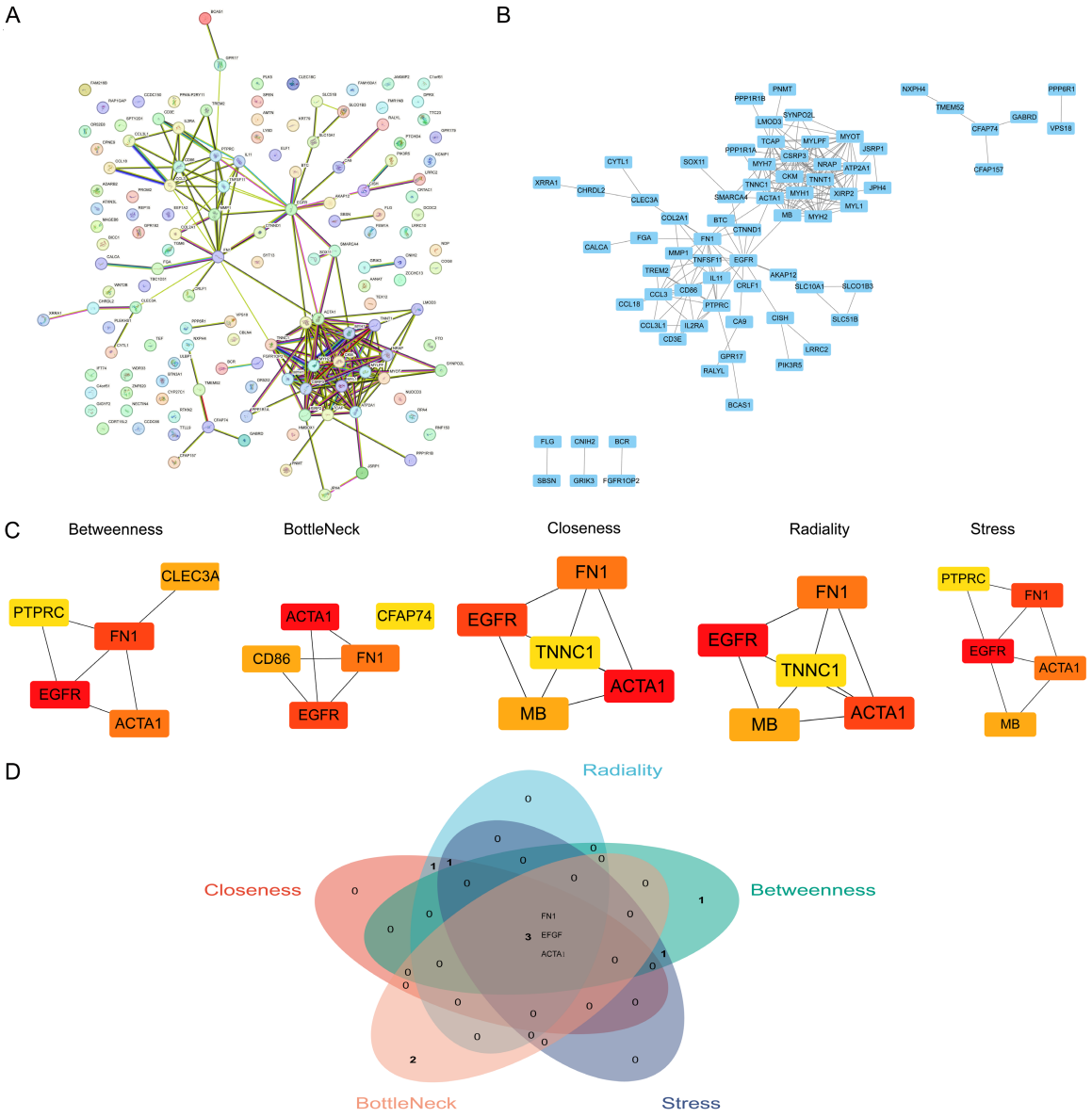

Figure 4. PPI network construction and hub gene identification of DEGs. A. The PPI network of the 148 DEGs was constructed using the STRING database (confidence score > 0.7), resulting in a network comprising 138 nodes and 211 edges. Each node represents a protein encoded by a DEG, and each edge represents a protein-protein interaction. B. Visualization of the PPI network using Cytoscape software. The nodes (blue rectangles) represent the identified DEGs, and the edges represent the protein-protein interactions. C. Identification of hub genes using five methods (Closeness, Betweenness, Radiality, BottleNeck, and Stress) implemented in the cytoHubba plugin of Cytoscape. The top 5 hub genes identified by each method are displayed, with color gradients representing the ranking scores. D. Venn diagram showing the overlap of hub genes identified by the five algorithms. Three key hub genes (FN1, EGFR, and ACTA1) were consistently identified across all five algorithms, indicating their central roles in the PPI network and potential importance in OLF pathogenesis.

GSVA was performed to compare pathway activity at the individual sample level. GSVA identified multiple differentially activated pathways between groups (**Figure 3H**), including glycolysis, protein secretion, PI3K/AKT/mTOR signaling, mitotic spindle, inflammatory response, xenobiotic metabolism, heme metabolism, hypoxia, androgen response, spermatogenesis, and IL6/JAK/STAT3 signaling.

PPI interaction network construction and hub gene identification

To identify key hub genes in OLF pathogenesis, a PPI network was constructed using the

Table 4. Key central hub genes of the primary connected component

Gene name	Closeness Centrality	Betweenness Centrality	Radiality	BottleNeck	Stress
FN1	0.508	0.372	0.951	1.968	4860
EGFR	0.512	0.405	0.952	1.952	4562
ACTA1	0.496	0.265	0.949	2.015	3960

STRING database with a confidence score threshold of ≥ 0.7. The resulting network comprised 138 nodes and 211 edges (**Figure 4A**), which was visualized using the Cytoscape software (**Figure 4B**). Hub genes were systematically identified using five complementary centrality algorithms (Closeness, Betweenness, Radiality, BottleNeck, and Stress) implemented in the cytoHubba plugin. These algorithms assess different aspects of network topology: Closeness measures proximity to all nodes, Betweenness quantifies bridging importance, Radiality evaluates network centrality, BottleNeck identifies module connectors, and Stress measures pathway load. The top 5 hub genes from each algorithm were selected (**Figure 4C**). Intersection analysis using a Venn diagram revealed three core hub genes - FN1 (fibronectin 1), EGFR (epidermal growth factor receptor), and ACTA1 (actin alpha 1) - that were consistently ranked among the top 5 across all five algorithms (**Figure 4D**). The detailed centrality metrics for these hub genes are presented in **Table 4**. FN1 showed high scores across all metrics (Closeness = 0.508, Betweenness = 0.372, Radiality = 0.951, BottleNeck = 1.968, Stress = 4860), EGFR exhibited the highest closeness (0.512) and betweenness (0.405) centrality, and ACTA1 demonstrated substantial centrality scores with the highest BottleNeck value (2.015). These hub genes represent key molecular players in OLF: FN1 is involved in ECM remodeling, EGFR mediates growth factor signaling and cellular proliferation, and ACTA1 reflects the disruption of normal tissue architecture. Their consistent identification across multiple algorithms strongly supports their central importance in OLF pathogenesis.

Immune cell infiltration and immune correlation analysis

To characterize the immune microenvironment in OLF, we employed CIBERSORT to quantify 22 distinct immune cell types in OLF and non-OLF samples. The immune cell composition for each sample is shown in **Figure 5A**. Comparative analysis revealed that resting dendritic cells were significantly elevated in OLF tissues ($P < 0.05$), while M1 macrophages and eosinophils were significantly decreased ($P < 0.05$) (**Figure 5B**), indicating a distinct immune infiltration pattern in OLF. Correlation analysis among the 22 immune cell types (**Figure 5C**) revealed strong positive correlations between naive B cells and plasma cells ($r > 0.8$, $P < 0.01$), CD4 memory resting T cells and follicular helper T cells ($r > 0.75$, $P < 0.01$), gamma delta T cells with resting NK cells and neutrophils ($r > 0.7$, $P < 0.05$), and resting mast cells with M0 macrophages and activated mast cells ($r > 0.65$, $P < 0.05$). In contrast, memory B cells and resting mast cells showed the weakest correlations ($r < 0.2$, $P > 0.05$).

To investigate the roles of the hub genes in immune modulation, we performed correlation analysis between FN1, EGFR, ACTA1 expression and immune cell infiltration. FN1 showed significant positive correlations with M0/M2 macrophages, resting dendritic cells ($r = 0.94$, $P < 0.01$), and mast cells, while negatively correlating with B cells, monocytes, activated dendritic cells, and eosinophils ($r = -0.76$, $P < 0.05$) (**Figure 6A-C**). ACTA1 exhibited an opposite pattern, positively correlating with B cells, monocytes, and activated dendritic cells, but negatively correlated with macrophages, resting dendritic cells ($r = -0.81$, $P < 0.05$), and mast cells (**Figure 6A**, **6F**). EGFR was found to be positively correlated with B cells, plasma cells, resting NK cells, and eosinophils ($r = 0.88$, $P < 0.01$), while negatively correlating with macrophages, resting dendritic cells ($r = -0.95$, $P < 0.01$), and mast cells (**Figure 6A**, **6D**, **6E**). These findings demonstrate that the three hub genes are intricately linked to immune cell regulation in OLF, with FN1 and ACTA1 showing opposing correlation patterns, suggesting their coordinated roles in modulating the immune microenvironment during ligamentum flavum ossification.

Discussion

The present study provided a comprehensive bioinformatic characterization of gene expres-

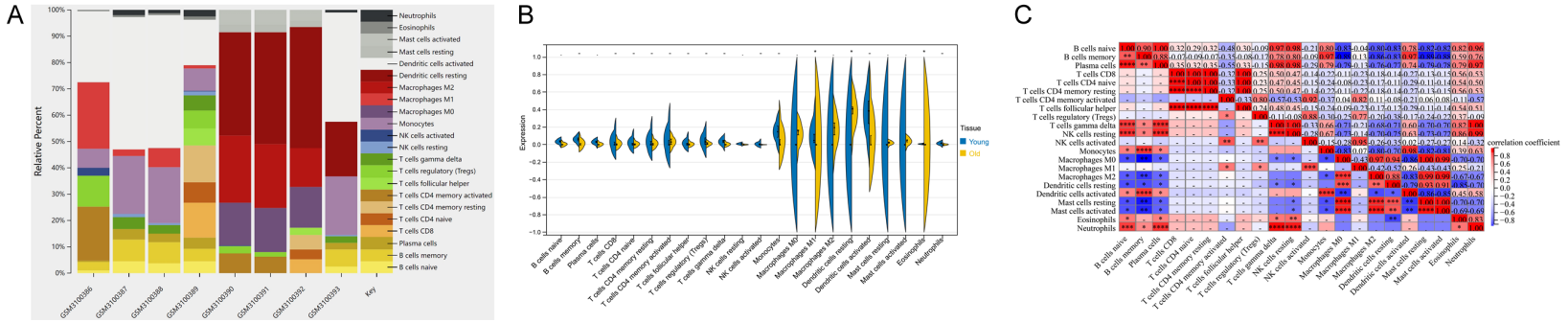

Figure 5. Immune infiltration analysis in OLF and non-OLF samples using the CIBERSORT method. A. Bar plot displays the estimated proportions of 22 distinct immune cell types within the tissue microenvironment of each OLF and non-OLF sample. B. A comparison analysis of immune cell distribution between the OLF and non-OLF samples revealed several significantly altered populations. Specifically, resting dendritic cells showed a higher infiltration level in OLF samples, while the proportions of M1 macrophages and eosinophils were significantly lower in the OLF group. C. Correlation analysis among the 22 immune cell types showed strong positive associations between cell subsets, such as naive B cells and plasma cells, as well as resting memory CD4 T cells and follicular helper T cells. Conversely, memory B cells and resting mast cells exhibited the weakest correlations across the samples.

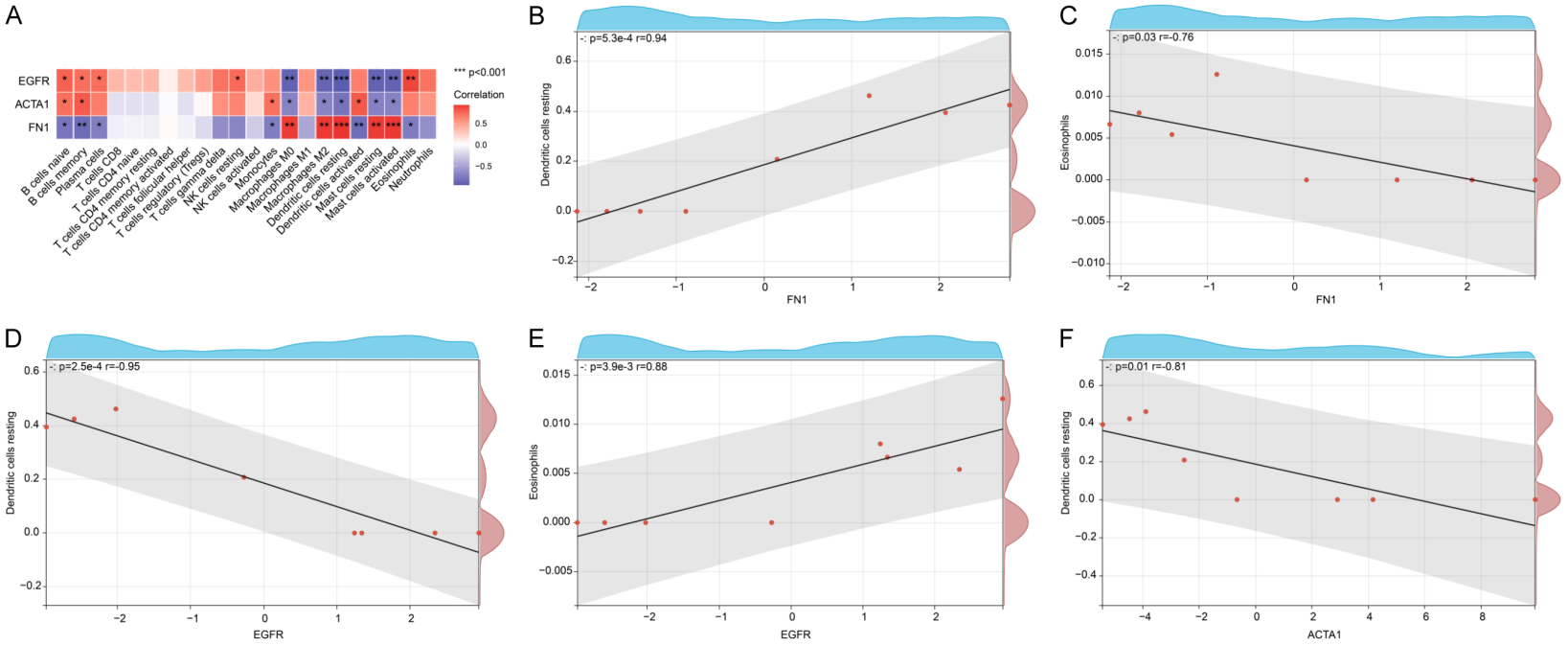

Figure 6. Correlation analysis between hub genes and immune cell infiltration in OLF Samples. (A) Heatmap illustrating correlations between hub genes (FN1, ACTA1, and EGFR) and 22 immune cell types. Notably, FN1 is positively correlated with M0 and M2 macrophages, and resting dendritic cells, while negatively correlated with B cells and eosinophils. ACTA1 shows opposite correlation patterns to FN1. EGFR is positively correlated with B cells and eosinophils, while negatively correlated with macrophages and resting dendritic cells. (B-F) Scatter plots with linear regression lines displaying specific significant associations: (B) Positive correlation between FN1 and resting dendritic cells, (C) Negative correlation between FN1 and eosinophils, (D) Negative correlation between EGFR and resting dendritic cells, (E) Positive correlation between EGFR and eosinophils, and (F) Negative correlation between ACTA1 and resting dendritic cells.

sion profiles in OLF, revealing key molecular mechanisms and pathways possibly contributing to disease pathogenesis. We identified 148 DEGs distinguishing OLF from non-OLF tissues, with functional enrichment analysis revealing a predominant involvement in muscle contraction and immune response processes. By integrating PPI network construction and immune cell infiltration analysis, we delineated a critical regulatory network driven by FN1, EGFR and ACTA1. These findings suggest a mechanism linking ECM remodeling, fibrotic transformation, and immune dysregulation in the pathology of OLF.

Functional enrichment analyses demonstrated that OLF is closely associated with muscle contraction-related processes, as evidenced by significant enrichment of DEGs in GO terms including muscle filament sliding, sarcomere organization, and actin binding. These findings suggest that the mechanical properties and contractile apparatus of the ligamentum flavum undergo substantial alterations in OLF, which may contribute to tissue stiffening and subsequent ossification. This aligns with previous biomechanical and histological studies, which have demonstrated that repetitive mechanical stress and the degeneration of elastic fibers can accelerate hypertrophy and calcification of the ligamentum flavum, thereby predisposing to ectopic bone formation [8, 9, 36]. Our results are consistent with these observations and further indicate that the dysregulation of muscle- and cytoskeleton-related genes represents a pivotal upstream event in the structural remodeling of the ligamentum flavum.

In addition, KEGG pathway analysis highlighted the involvement of immune-related pathways, including cytokine-cytokine receptor interactions and viral protein interactions with cytokines, while GSEA revealed significant enrichment of epithelial-mesenchymal transition (EMT) (NES = 2.05, FDR < 0.001), glycolysis, and inflammatory response pathways in OLF samples. Previous studies have reported increased expression of osteogenic markers (e.g., RUNX2, osteocalcin, and alkaline phosphatase) and elevated levels of pro-inflammatory cytokines (e.g., TNF-α, IL-6, and IL-1β) in ossified ligamentum flavum specimens [16, 37, 38], supporting the concept that chronic inflammation and dysregulated tissue remodeling jointly promote endochondral ossification. Our findings are in line with these observations and extend the current understanding by suggesting that metabolic reprogramming (glycolysis and cholesterol homeostasis) and inflammatory activation may act in concert to drive the critical transition from ligament hypertrophy to ossification. The coordinated activation of EMT, glycolysis, and inflammatory pathways suggests a fundamental shift in cellular metabolism that supports the energy demands of actively proliferating cells involved in ectopic bone formation.

The identification of FN1, EGFR, and ACTA1 as hub genes within the PPI network suggests that these genes may serve as central regulators in the progression of OLF. These genes are recognized as potent drivers of fibrosis, governing cell adhesion, cytoskeletal organization, and signal transduction [39-41]. Functionally, FN1 regulates the ECM microenvironment to facilitate cell adhesion and migration [42], while ACTA1, drives excessive ECM accumulation via myofibroblast differentiation and actin cytoskeleton dynamics [41]. Concurrently, EGFR signaling mediates cell survival and proliferation, further exacerbating fibrotic responses [43]. Together, these proteins form a critical network that drives the pathological progression of fibrosis in the ligamentum flavum. Their high connectivity within our PPI network suggests that they act as upstream regulators, coordinating a complex interplay of ECM deposition and cytoskeletal remodeling that ultimately fuels ligament hypertrophy and ectopic ossification.

Immune cell infiltration analysis further revealed that FN1, EGFR, and ACTA1 are intricately linked to distinct immune cell populations within the OLF microenvironment. Specifically, FN1 expression exhibited a significant positive correlation with M0 and M2 macrophages, resting dendritic cells, and mast cells, while showing a negative correlation with B-cell subsets, monocytes, and eosinophils. Conversely, ACTA1 and EGFR displayed distinct yet overlapping correlation profiles with naive and memory B cells, monocytes, dendritic cells, NK cells, and macrophages. These findings are in line with previous reports suggesting that macrophage polarization, mast cell activation and B-cell responses are pivotal drivers of chronic inflammation and tissue remodeling in heterotopic ossification [44-46]. The observed interplay between these hub genes and immune cell dynamics suggests a multifaceted mechanism in which fibrotic and immune processes reinforce each other in OLF. By integrating PPI network analysis with immune infiltration profiling, our work extends previous studies that primarily focused on osteogenic differentiation and classical signaling pathways (such as BMP/TGF-β and Wnt/β-catenin) [8, 18], and provides a broader immunogenomic perspective on OLF pathogenesis.

Several limitations of this study should be acknowledged. First, our analysis was based on a single public microarray dataset with a relatively small sample size (four OLF and four non-OLF samples), which may have constrained the statistical power and generalizability of the findings. Second, the dataset comprised specimens with ligamentum flavum hypertrophy rather than radiologically or pathologically confirmed ossification. While hypertrophy is widely recognized as a critical precursor state to ossification, implying a shared pathologic continuum, our results may specifically reflect the early or transitional molecular events of the disease rather than the full transcriptomic landscape of terminal ossification. Third, this study is purely bioinformatic and exploratory in nature; the predicted hub genes, pathways, and immune cell infiltration patterns have not yet been validated experimentally. Despite these limitations, our findings provide a valuable foundation for future research. Future studies with larger, independent cohorts and integrated multi-omics analyses, combined with *in vitro* and *in vivo* functional experiments, are needed to confirm the roles of FN1, EGFR, and ACTA1 in the progression of OLF and to evaluate their clinical use as diagnostic biomarkers or therapeutic targets.

Acknowledgements

The project was supported by the Shandong Provincial National Natural Science Foundation (ZR2022MH046).

Disclosure of conflict of interest

None.

Address correspondence to: Dr. Changliang Peng, Department of Spinal Surgery, The Second Qilu Hospital of Shandong University, No. 247, Beiyuan Street, Jinan 250033, Shandong, China. Tel: +86-187-5310-7090; Fax: +86-531-85875480; E-mail: pcliang@sdu.edu.cn

References

[1] Lin CR, Tsai SHL, Yu TW, Lin PC, Tsai ZD, Lee KH, Fu TS, Lai PL, Tsai TT and Hu YH. Open posterior approach versus endoscopic approach for thoracic ligamentum flavum ossification: a systematic review and meta-analysis. Eur Spine J 2025; 34: 380-403.

[2] Chen G, Fan T, Yang X, Sun C, Fan D and Chen Z. The prevalence and clinical characteristics of thoracic spinal stenosis: a systematic review. Eur Spine J 2020; 29: 2164-2172.

[3] Daniels AH, McDonald CL, Basques BA and Kuris EO. Ossified ligamentum flavum: epidemiology, treatment, and outcomes. J Am Acad Orthop Surg 2022; 30: e842-e851.

[4] Zhao Y, Xiang Q, Jiang S, Wang L, Lin J, Sun C and Li W. Prevalence, diagnosis, and impact on clinical outcomes of dural ossification in the thoracic ossification of the ligamentum flavum: a systematic review. Eur Spine J 2023; 32: 1245-1253.

[5] Xin Z, Kong W, Cai M, Du Q, Liu L, He J, Qin J, Wang A, Ao J and Liao W. Translaminar osseous channel-assisted full-endoscopic flavectomy decompression of thoracic myelopathy caused by ossification of the ligamentum flavum: surgical technique and results. Pain Physician 2020; 23: E475-E486.

[6] Nie C, Chen K, Gu S, Lyu F, Jiang J, Xia X and Zheng C. Hybrid decompression-based surgical strategy for treating multilevel thoracic ossification of the ligamentum flavum: a retrospective study. Asian Spine J 2025; 19: 74-84.

[7] Wang Y, Tang Z, Tang Q, Ma H, Shen M and Yang H. Comparison of the clinical efficacy and

safety of two spinal endoscopic techniques for the treatment of ossification of the ligamentum flavum in the thoracic spine. Front Neurol 2025; 16: 1630315.
[8] Silwal P, Nguyen-Thai AM, Alexander PG, Sowa GA, Vo NV and Lee JY. Cellular and molecular mechanisms of hypertrophy of ligamentum flavum. Biomolecules 2024; 14: 1277.
[9] Zhang C, Chang Y, Shu L and Chen Z. Pathogenesis of thoracic ossification of the ligamentum flavum. Front Pharmacol 2024; 15: 1496297.
[10] Chen KZ, Lin ZY, Chen LJ, Zhou YX, Zhang W, Wan HY, Huo YK, Fu Q, Gao ZQ, Cheng HW, Ma XD and Zhang SS. TNC-targeted CAR-macrophage therapy alleviates liver fibrosis in mice. Mil Med Res 2025; 12: 78.
[11] Huang E, Peng N, Xiao F, Hu D, Wang X and Lu L. The roles of immune cells in the pathogenesis of fibrosis. Int J Mol Sci 2020; 21: 5203.
[12] Zhao Y, Xiang Q, Jiang S, Lin J and Li W. Revealing the novel metabolism-related genes in the ossification of the ligamentum flavum based on whole transcriptomic data. JOR Spine 2024; 7: e1357.
[13] Liu Y, Li Y, Liu Y, Gao Z, Zhang J, Qiu Y, Wang C, Lu X and Yang J. Investigation of the shared biomarkers in heterotopic ossification between ossification of the ligamentum flavum and ankylosing spondylitis. Global Spine J 2025; 15: 161-174.
[14] Dou X, Mao T, Ma Y, Jia F, Liu Y and Liu X. Fibrotic and inflammatory characteristics of epidural fat adjacent to the ossification area in patients with ossification of the ligament flavum. JOR Spine 2022; 5: e1229.
[15] Yang J, Chen G, Fan T and Qu X. M1 macrophage-derived oncostatin M induces osteogenic differentiation of ligamentum flavum cells through the JAK2/STAT3 pathway. JOR Spine 2023; 7: e1290.
[16] Jiang C, Wang W, Chen YL, Chen JH, Zhang ZW, Li J, Yang ZC and Li XC. Macrophage polarization and macrophage-related factor expression in hypertrophy of the ligamentum flavum. Eur Spine J 2024; 33: 4476-4487.
[17] Qu X, Xu G, Hou X, Chen G, Fan T, Yang X and Chen Z. M1 macrophage-derived interleukin-6 promotes the osteogenic differentiation of ligamentum flavum cells. Spine (Phila Pa 1976) 2022; 47: E527-E535.
[18] Ham CH, Kim Y, Kwon WK, Sun W, Kim JH, Kim HJ and Moon HJ. Single-cell analysis reveals fibroblast heterogeneity and myofibroblast conversion in ligamentum flavum hypertrophy. Spine J 2025; 25: 1263-1275.
[19] Mishra S, Singh S, Ashish A, Rai S and Singh R. Unveiling immune and signalling proteins in recurrent pregnancy loss: GEO2R analysis sheds light. Comput Biol Med 2025; 194: 110535.
[20] Ikuta M, Kaito T, Fujimori T, Kitahara T, Furuichi T, Bun M, Hirai H, Ukon Y, Kanie Y, Takenaka S and Okada S. Review of basic research about ossification of the spinal ligaments focusing on animal models. J Clin Med 2023; 12: 1958.
[21] Sun C, Zhang H, Wang X and Liu X. Ligamentum flavum fibrosis and hypertrophy: molecular pathways, cellular mechanisms, and future directions. FASEB J 2020; 34: 9854-9868.
[22] Aleksić V, Todorović J, Miladinović N, Aleksić N, Bogosavljević V, Đurović M, Kocić S, Aleksić R and Joković M. Ligamentum flavum analysis in patients with lumbar discus hernia and lumbar spinal stenosis. Sci Rep 2023; 13: 3804.
[23] Zhao Y, Xiang Q, Tian S, Wu Z, Lin J, Wang L, Sun Z and Li W. Noncoding RNA as a crucial epigenetic modulator in the degeneration of the ligamentum flavum. Exp Mol Med 2024; 56: 2551-2558.
[24] Zhang Y, Zhang X, Guo J, Dai W, Chen S, Huang L, Xiang X, Yu W and Su D. Stressors-induced cognitive dysfunction during aging: mechanisms and future challenges. Front Aging Neurosci 2025; 17: 1630982.
[25] Shi J, Zhang YQ, Hao DD, Fu SH and Meng JL. Key regulatory genes and signaling pathways involved in islet culture: a bioinformatic analysis. Int J Clin Exp Pathol 2021; 14: 292-303.
[26] Hale AT, He J, Larkin GM, Bastarache L and Isaacs AM. Genetically determined alterations in inflammation and infection-associated genes are associated with hydrocephalus in patients of African ancestry. Neurosurgery 2025; [Epub ahead of print].
[27] Gao M, Kong W, Huang Z and Xie Z. Identification of key genes related to lung squamous cell carcinoma using bioinformatics analysis. Int J Mol Sci 2020; 21: 2994.
[28] Gao Q, Fan L, Chen Y and Cai J. Identification of the hub and prognostic genes in liver hepatocellular carcinoma via bioinformatics analysis. Front Mol Biosci 2022; 9: 1000847.
[29] Sun Y, Han L and Sun D. Comprehensive analysis of EML2 as a prognostic biomarker in colon cancer. Int J Clin Exp Pathol 2024; 17: 1-12.
[30] Wang B, van der Kloet F, Kes MBMJ, Luirink J and Hamoen LW. Improving gene set enrichment analysis (GSEA) by using regulation directionality. Microbiol Spectr 2024; 12: e0345623.
[31] Liu C, Qu Z, Zhao H, Wang P, Zhan C and Zhang Y. Pan-cancer analysis of SYNGR2 with a focus on clinical implications and immune landscape in liver hepatocellular carcinoma. BMC Bioinformatics 2023; 24: 192.
[32] Wang H, Ji X, Chen L, Ju L, Ma Q, Wu Y and Cai W. Semaphorin4F is a potential biomarker for clinical progression and prognosis in gastric cancer. Int J Clin Exp Pathol 2023; 16: 210-224.

[33] Chen JJ, Lu ZZ, Jing YX, Nong XM, Qin Y, Huang JY, Lin N and Wei J. CD79A and GADD45A as novel immune-related biomarkers for respiratory syncytial virus severity in children: an integrated machine learning analysis and clinical validation. Front Immunol 2025; 16: 1609183.
[34] Lu Q, Jiang Y, Cang X, Pan J, Shen X, Tang R, Zhou Z and Zhu Y. Study of the immune infiltration and sonic hedgehog expression mechanism in synovial tissue of rheumatoid arthritis-related interstitial lung disease under machine learning CIBERSORT algorithm. Mol Biotechnol 2025; 67: 3217-3233.
[35] Shen W, Song Z, Zhong X, Huang M, Shen D, Gao P, Qian X, Wang M, He X, Wang T, Li S and Song X. Sangerbox: a comprehensive, interaction-friendly clinical bioinformatics analysis platform. Imeta 2022; 1: e36.
[36] Ye Z, Yin X, Ao J, Qin J, Wei Z and Qian H. Biological mechanisms underlying the ossification of ligamentum flavum and potential therapeutic targets derived from current research. Eur Spine J 2025; 34: 2926-2943.
[37] Huang AY, Shu L, Chen Z and Zhang C. IL-6 is involved in thoracic ossification of the ligamentum flavum. PLoS One 2022; 17: e0272357.
[38] Guo H, Yang L, Liu J, Chen L, Huang Y and Li J. KLF5 promotes the ossification process of ligamentum flavum by transcriptionally activating CX43. J Orthop Surg Res 2024; 19: 244.
[39] Resnikoff HA and Schwarzbauer JE. Increased basal fibronectin is sufficient to promote excess endothelial cell matrix assembly causing localized barrier dysfunction. Mol Biol Cell 2024; 35: ar120.
[40] Chiusa M, Hu W, Zienkiewicz J, Chen X, Zhang MZ, Harris RC, Vanacore RM, Bentz JA, Remuzzi G, Benigni A, Fogo AB, Luo W, Mili S, Wilson MH, Zent R, Hawiger J and Pozzi A. EGF receptor-mediated FUS phosphorylation promotes its nuclear translocation and fibrotic signaling. J Cell Biol 2020; 219: e202001120.
[41] Aujla PK, Hu M, Hartley B, Kranrod JW, Viveiros A, Kilic T, Owen CA, Oudit GY, Seubert JM, Julien O and Kassiri Z. Loss of ADAM15 exacerbates transition to decompensated myocardial hypertrophy and dilation through activation of the calcineurin pathway. Hypertension 2023; 80: 97-110.
[42] Tan X, Liu Z, Wang Y, Wu Z, Zou Y, Luo S, Tang Y, Chen D, Yuan G and Yao K. miR-138-5p-mediated HOXD11 promotes cell invasion and metastasis by activating the FN1/MMP2/MMP9 pathway and predicts poor prognosis in penile squamous cell carcinoma. Cell Death Dis 2022; 13: 816.
[43] Cao S, Pan Y, Terker AS, Arroyo Ornelas JP, Wang Y, Tang J, Niu A, Kar SA, Jiang M, Luo W, Dong X, Fan X, Wang S, Wilson MH, Fogo A, Zhang MZ and Harris RC. Epidermal growth factor receptor activation is essential for kidney fibrosis development. Nat Commun 2023; 14: 7357.
[44] Liu H, Li X, Li M, Sun Z, Wang X, Li J, Xu B, Chen Q, Fan C and Ruan H. POSTN-mediated interplay of M1 polarized macrophage with tendon-derived stem cells to drive traumatic heterotopic ossification formation through PTK7/ATK signaling? Adv Sci (Weinh) 2025; 12: e07951.
[45] Jiang T, Ao X, Xiang X, Zhang J, Cai J, Fu J, Zhang W, Zheng Z, Chu J, Huang M, Zhang Z and Wang L. Mast cell activation by NGF drives the formation of trauma-induced heterotopic ossification. JCI Insight 2024; 10: e179759.
[46] Yang HZ, Zhan Y, Liu Y, Guo M, Fan Y, Luo G, Zhao Y, Huang S, Sun T, Li SS, Ye Q and Jin X. NIR-stimulated rGO-HAMC hydrogel enhances fracture healing through regulating B-cell signaling. Biomater Adv 2025; 166: 214080.